JACS
JOURNAL OF THE AMERICAN CHEMICAL SOCIETY
Communication
pubs.acs.org/JACS

Gas Permeation in a Molecular Crystal and Space Expansion

Yuichi Takasaki and Satoshi Takamizawa*

Department of Nanosystem Science, Graduate School of Nanobioscience, Yokohama City University, 22-2 Seto, Kanazawa-ku, Yokohama, Kanagawa 236-0027, Japan

Supporting Information

ABSTRACT: A novel single-crystal membrane $[Cu(II)_2(4\text{-F-bza})_4(2\text{-mpyz})]_n$ (4-F-bza = 4-fluorobenzoate; 2-mpyz = 2-methylpyrazine) was synthesized and its identical permeability in any crystal direction in the correction for tortuosity proved that gas diffuses inside the channels without detour. H_2 permeated by 1.18×10^{-12} mol m m^{-2} s^{-1} Pa^{-1} with a high selectivity ($F\alpha$: 23.5 for H_2/CO and 48.0 for H_2/CH_4) through its 2D-channels having a minimum diameter of 2.6 Å, which is narrower than the Lennard-Jones diameter of H_2 (2.827 Å), CO (3.690 Å), and CH_4 (3.758 Å). The high rate of permeation was well explained by a modified Knudsen diffusion model based on the space expansion effect, which agrees with the observed permselectivity enhanced for smaller gases in considering the expansion of a channel resulting from the collision of gas molecules or atoms onto the channel wall. An analysis of single-crystal X-ray data showed the expansion order to be H_2 > Ar > CH_4, which was expected from the permeation analysis. The permselectivity of a porous solid depends on the elasticity of the pores as well as on the diameter of the vacant channel and the size of the target gas.

Membrane separation is one of the most basic separation techniques used in pure and applied science. It is highly regarded for its advantages in operation simplicity and energy expendability.[1,2] Microporous materials are attractive materials for the adsorption or separation of gases. In particular, hydrogen is one of the important gas species in industry,[3] and the efficient purification of H_2 gas is a highly attractive target in membrane gas separation. A pore whose size is near that of the target gas particle offers high selectivity but sacrifices permeability at the same time.[4] To overcome this problem, enhancement of the affinity between the target gas and the pores by mixing polycrystalline MOFs into the substrate membrane has been studied.[5] Although some sort of novel material design is essential for improving both permeability and selectivity,[6] the complexity of membranes such as polymer membranes,[7] inorganic polycrystalline membranes,[8] which possess durability and formability, would hamper finding obvious solutions in the design of permselective materials because of their unknown qualities and disarray in a structural sense. Since microporous single-crystal membranes have regular and homogeneous pores with extremely low defects and no boundaries, the plural types of similar single crystals only with different pore structures could possibly point to important knowledge for improving permselectivity related to pore structure. We have already reported anisotropic gas permeation along the channel running layer of $[Cu(II)_2(bza)_4(pyz)]_n$ (**2**) (bza = benzoate; pyz = pyrazine) with relatively high permeability compared with conventional zeolite single-crystal membrane.[9,10] In this study, we have succeeded in preparing a novel single-crystal membrane of a newly synthesized porous metal complex $[Cu(II)_2(4\text{-F-bza})_4(2\text{-mpyz})]_n$ (**1**)[11] as a derivative of **2**[12] and investigated the gas permeation behavior of **1**. By considering the correlation between pore structure and gas permeation behavior using the single-crystal membranes of **1** and **2**, we encountered an unknown mechanism of permeation where diffusion of the relatively smaller gas is accelerated.

The crystal structure of **1** (monoclinic, $C2/m$)[13] is gathered by 1D chains in which the paddle-wheel units (binuclear Cu_2 center with four 4-F-bza) are bridged by 2-mpyz, taking essentially the same structure of **2** (monoclinic, $C2/c$), but the channel geometry of **1** is different from that of **2**. In **1**, the packing structure was formed through $\pi-\pi$ interaction between two phenyl rings along the c axis and CF$-\pi$ interaction between a fluorine atom and pyrazine ring along the a axis to generate 2D-channel networks spreading over the ab plane along [110] and [−110] by connection of void spaces at their four corners as a neck moiety, while the channel of **2** runs parallel with the ab plane along [110] or [1−10] to form a nearly straight cylinder (yellow region in Figure 1b,d). The widest channel diameters (d^{max}), which were measured between the van der Waals surface of the channel walls constructed by phenyl rings, are almost same as 8.1 Å for **1** and 8.2 Å for **2**, but the narrowest channel diameters (d^{min}) are obviously different, as the values are 2.6 Å for **1** and 5.5 Å for **2**. The value of d^{min} for **1** (d_1^{min}) is slightly smaller than the Lennard-Jones diameter[14] of H_2 (σ_{H2} = 2.827 Å), while that for **2** (d_2^{min}) is larger than the diameter of CH_4 (σ_{CH4} = 3.758 Å). Therefore, high selectivity with low diffusivity for H_2 gas permeation was expected in the crystal membrane of **1**.

In the gas permeation measurements, the single-crystal membrane of **1** showed moderate gas permeation properties for all gases used in this study (He, H_2, CO_2,[15] O_2, Ar, CO, CH_4, and N_2) in contrast to the prior expectation of low diffusivity based on the narrow channel structure that was confirmed by X-ray diffraction analysis. Although d_1^{min} (2.6 Å) is narrower than the diameter of H_2 (σ_{H2} = 2.827 Å), the observed permeability values along [100] direction were high for H_2 with 1.18×10^{-12} mol m m^{-2} s^{-1} Pa^{-1}, which is almost the same value of **2** for H_2 as 1.11×10^{-12} mol m m^{-2} s^{-1} Pa^{-1}, and moderate for larger gases such as CO and CH_4 (σ_{CO} = 3.690 Å, σ_{CH4} = 3.758 Å) with 5.03×10^{-14} mol m m^{-2} s^{-1} Pa^{-1} for CO and 2.46×10^{-14} mol m m^{-2} s^{-1} Pa^{-1} for CH_4 (Figure 1e). The ideal selectivity ($F\alpha$) for H_2/

Received: January 31, 2014
Published: April 30, 2014

ACS Publications © 2014 American Chemical Society

dx.doi.org/10.1021/ja501045u | J. Am. Chem. Soc. 2014, 136, 6806−6809

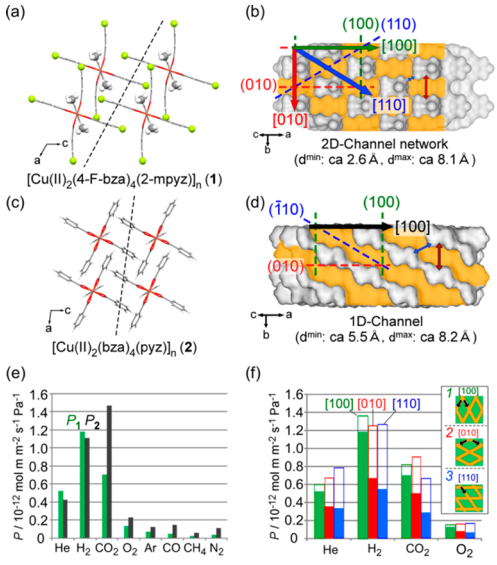

Figure 1. (a, c) Packing structures of **1** and **2** with light green and gray spherical model for fluorine atoms and methyl groups, respectively, at 90 K. (b, d) Cross-sections of crystal structures as solvent-accessible model illustrated along dotted line in (a) and (c). Yellow regions are void spaces; colored single-headed arrows are gas permeation directions. The widest and narrowest positions in the channel are represented as red and blue double-headed arrows. (e) Permeability along [100] direction for **1** (green) and **2** (black) at 293 K and 150 kPa. (f) Dependence of crystal orientations on permeability of **1**. [100]: green, [010]: red, [110]: blue. Blank parts of each bar represent increasing value by adopting τ and ε. (τ is 1.16, 1.99, and 1.15 for orientations *1*, *2*, and 3, respectively; ε is 0.132 for *1* and *2*, respectively, and 0.066 for *3*.)

CO or H_2/CH_4 of **1** were estimated as being 2.5−3 times higher than those of **2** ($F\alpha_1$ = 23.5 and $F\alpha_2$ = 7.45 for H_2/CO, $F\alpha_1$ =48.0 and $F\alpha_2$ = 19.0 for H_2/CH_4, respectively). The higher $F\alpha$ for H_2 of **1** compared to those of **2** agreed with the prior expectation based on the channel narrowness of **1**. Surprisingly, performance enhancement in H_2 permselectivity was achieved without any decrease of H_2 permeability, leading to the necessity of removing the possibility of the presence of some shortcut pathways other than channels before getting an accurate analysis for gas permeation.

First, we ascertained where the gases diffuse in the crystal membrane based on the Knudsen diffusion model, which represents the behavior of diluted gas permeation through a cylindrical space as eq 1,[16] since we demonstrated the qualitative validation of the model for the gas permeation of **2** in a previous report[10]

$$P_i = \frac{1}{3}\frac{\varepsilon_i}{\tau_i} d_i \sqrt{\frac{8RT}{\pi M}} \frac{\Delta C_{0i}}{\Delta p} \quad (1)$$

where ε is porosity, τ is tortuosity (l_d/l_s: ratio of pathway length, l_d, versus membrane thickness, l_s), d is channel diameter, R is gas constant, T is absolute temperature (293 K), M is molecular weight, ΔC_{0i} is differential gas concentration between top and back of membrane under a static state, Δp is differential pressure (150 kPa), and i denotes the crystal membrane of **1** or **2**. According to eq 1, permeability should depend on channel geometry as well as on channel diameter, gas species, and gas concentration in the channel. If the gas diffuses inside the channel, the contribution of channel geometry to permeability can be extracted by changing the crystal orientation of **1** because, in principle, the other parameters are invariant for any orientations of the same membrane. The permeability values for He, H_2, CO_2, and O_2 gases along [100], [010], and [110] directions (orientations *1*−*3*), which were the most effective in this experiment, were collected. The observed permeability values in orientations *2* and *3* were almost half that of orientation *1*. The values in each orientation became identical after the terms of tortuosity and porosity calculated from the X-ray crystal structure of **1** were adopted. This result clearly demonstrated that each gas actually diffuses inside the channels of **1** without detour from the channel in crystal structural analysis. (The gas barrier property was confirmed along the [001] direction (Table S7).)

In order to understand the relationship between gas permeability and channel diameter, we introduced index f, which is the permeability ratio (P_1/P_2) of the membrane of **1** and **2** divided by the gas concentration ratio ($\Delta C_{01}/\Delta C_{02}$) for each permeate gas (see eq 2). In this treatment, the chemical properties of an individual gas can be offset by taking the ratio with the same gas species. ΔC_0 can be substituted by the equilibrium gas concentration determined in gas adsorption measurements under the same conditions of the gas permeation experiments with 150 kPa at 293 K (Figure S3, Supporting Information (SI))

$$f = \left(\frac{P_1}{P_2}\right)\left(\frac{\Delta C_{01}}{\Delta C_{02}}\right)^{-1} \quad (2)$$

The observed index values of f_{obs} showed a monotonic decreasing fashion with an increase of σ in the order of He, H_2, CO_2, O_2, Ar, CO, CH_4, and N_2.[14,15,17] Therefore, f can be a function of σ. If this deviation only relates to each channel diameter, the large value of f_{obs} (σ_{H2}) requires a channel in **1** that is 3 times wider, but in order to describe the decreasing curve as $f(\sigma)$, a variable for channel diameter that increases with a decrease in gas size in eq 1 is necessary. Therefore, we introduced assumption (i): In addition to the empty channel's diameter (d), the channel is widened by α and, taking the effective channel diameter ($d^*(\sigma)$),[18] which should deduct gas size from the widened channel diameter, effective porosity (ε^*)[18] and permeability ($P^*(\sigma)$) should also be corrected with the effective channel diameter.

$$P_i^*(\sigma) = \frac{1}{3\tau_i}\frac{\varepsilon_i(d_i+\alpha)^2}{d_i^2}[(d_i+\alpha)^2 - \sigma^2]^{1/2}\left(\frac{8RT}{\pi M}\right)^{1/2}\frac{\Delta C_{0i}}{\Delta p} \quad (1')$$

By introducing these effective parameters, the function of $f(\sigma)$ can be obtained.

In the replacement of d with d^{min},[19] adequate values of α = 1.25 Å (upper green curve in Figure 2a) and 4.6 Å (lower green curve in Figure 2a) are required for reproducing the experimental values of f_{obs} (σ_{N2}) and f_{obs} (σ_{H2}), respectively. Therefore, the magnitude of α with channel extension should be a decreasing function of σ. Therefore, we introduced the next assumption (ii): the local elongation of the channel diameter is caused by the collision of gas molecules onto the channel wall. The following equation was introduced for α as a function of σ in consideration of an elastic collision process

$$F = c\frac{\alpha(\sigma)}{2} = \frac{m\overline{v^2}}{3d} \quad \left(c = \frac{s}{d}E,\ p = \frac{F}{s} = \frac{4m\overline{v^2}}{3\pi d\sigma^2}\right) \quad (3)$$

$$\frac{\alpha(\sigma)}{2} = \frac{F}{s}\frac{d}{E} = \frac{m\overline{v^2}/3d}{\pi\sigma^2/4} = \frac{4k_BT}{\pi\sigma^2 E} \quad (4)$$

dx.doi.org/10.1021/ja501045u | J. Am. Chem. Soc. 2014, 136, 6806−6809

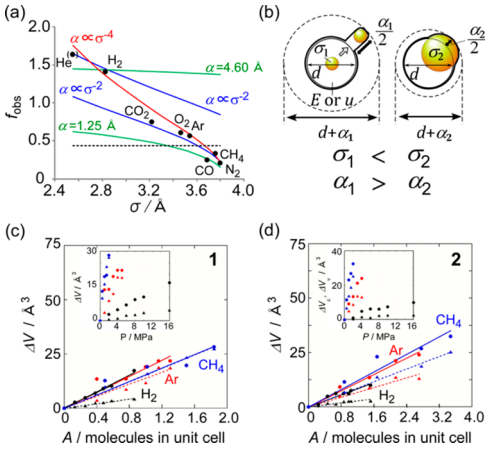

Figure 2. (a) Curve fittings to f_{obs} (black plots) by f_{calc} calculated from eqs 1 and 2 (black line), eqs 1′ and 2 (green curves), eqs 1′, 2, and 4 (blue curves), or eqs 1′, 2, and 6 (red curve), respectively. Parameters for the line and curves are d^{min} of 2.6 and 5.5 Å for **1** and **2**, $\tau_1 = 1.16$, $\tau_2 = 1.14$, $\varepsilon_1 = 1.32$, $\varepsilon_2 = 1.43$, $T = 293$ K, $E = 280$ MPa (upper blue curve) and 540 MPa (lower blue curve) and $u = 190$ MJ m^{-3} and 830 MJ m^{-3} for **1** and **2** (for red curve). (b) Relationship between σ and α in space expansion model. (c, d) Expanded volume in void (ΔV_v) as circle plots and in crystal lattice (ΔV_c) as triangle plots observed by X-ray diffraction under gas pressurized conditions of H_2 (black), Ar (red), and CH_4 (blue) for **1** and **2** against adsorption amount (A) at 293 K. Insets were plotted by pressure (MPa) as the horizontal axis. Void volume was calculated from a CIF in which the guest molecule was eliminated.

where s is the collision area ($\pi\sigma^2/4$) as a cross-section of a gas molecule, E is Young's modulus along the channel diameter of the space, F is force locally received on the channel wall from the collision of gas molecules, m is the mass of the gas molecules, p is gas pressure, $\langle v^2 \rangle$ ($= 3k_BT/m$) is the mean of the squared velocity of gas molecules estimated from kinetic theory, and k_B is the Boltzmann constant. We obtained the local elongation of the channel radius α (σ)/2 in eq 4 in consideration of the columnar deformation with the base area of the molecular cross section for a perpendicular collision onto the channel wall. (Refer to Figure 2b.) Although it should be noted that the value of Young's modulus changes with a change of channel diameter even in the same material in this account model, the values of $f_{calc}(\sigma)$ were close to the plots of f_{obs} except for f_{obs} (σ_{H2}) at $E = 540$ MPa (lower blue curve in Figure 2a), which is near the actual Young' modulus measured on a bulk single crystal of **1** and **2** along the normal direction for (001) as 108 and 223 MPa, respectively[20] (Figure S7, SI). However, the independently estimated magnitude of $E = 280$ MPa (upper blue curve in Figure 2a) was required in the curve fitting of f_{obs} (σ_{H2}) in eq 4. Consequently, our assumptions seem to be reasonable.

This elastic deformation model derives the proportional correlation of $f(\sigma)$ against σ^{-2}. However, the experimental f_{obs} could fit better if $f(\sigma)$ is proportional to σ^{-4}. This led to the volumetric energy model shown below.

$$u\Delta V = \frac{1}{2}m\overline{v^2} \quad \left(\Delta V = \frac{\alpha(\sigma)}{2}s\right) \tag{5}$$

$$\frac{\alpha(\sigma)}{2} = \frac{1}{2}\frac{F}{s}\frac{\pi d^3}{4}\frac{1}{us} = \frac{6k_BTd^2}{\pi\sigma^4 u} \tag{6}$$

where u is space-energy density of vacant space, ΔV is the expansion of space by local deformation of channel, and the space with smaller energy density means ease of channel deformation, as eq 5. We obtained the best fitted curve of $f_{calc}(\sigma)$ to f_{obs} over the entire range of σ with the parameters of $u = 190$ MJ m^{-3} and 830 MJ m^{-3} for **1** and **2**, respectively, by the least-squares method with eq 6 (red curve in Figure 2a).

To verify the channel expansion behavior caused by the presence of gas molecules in the channel, we performed a single-crystal X-ray structural analysis for H_2, Ar, and CH_4 inclusion under various gas pressures (up to 16 MPa) at 298 K. In the experiments, we monitored the expansion magnitude of void volume and crystal cell volume and clearly observed in linear an increase in the adsorption amount per unit cell (A) in both the void (ΔV_v) and also the crystal cell (ΔV_c). The gradient of ΔV_v vs A ($k_v = (\Delta V_v/A)$) was larger than that for ΔV_c vs A ($k_c = (\Delta V_c/A)$). This is caused by the competition between compression (inhibition of expansion) of the crystal cell by the surrounding gas pressure and channel expansion by gas inclusion. To simplify the complexity described above Δk ($= k_v - k_c$) in the amplitude of channel expansion was taken through the local deformation. The observed values of Δk for H_2 (**1**: 27.5 Å^3 molecule^{-1} and **2**: 19.0 Å^3 molecule^{-1}), Ar (**1**: 9.30 Å^3 molecule^{-1} and **2**: 15.0 Å^3 molecule^{-1}), and CH_4 (**1**: 0.20 Å^3 molecule^{-1} and **2**: 11.5 Å^3 molecule^{-1}) were near the expected expansion volumes of ($\alpha s/2$) in the gas permeation analysis discussed previously for H_2 (**1**: 13.4 Å^3 and **2**: 14.0), Ar (**1**: 8.52 Å^3 and **2**: 8.72), and CH_4 (**1**: 7.54 Å^3 and **2**: 7.82). The order of α in H_2 (**1**: 8.76 Å and **2**: 4.75 Å) > Ar (**1**: 1.48 Å and **2**: 2.39 Å) > CH_4 (**1**: 0.028 Å and **2**: 1.63 Å) calculated from k ($2/s$) were reasonable for the expectation from the permeation experimental analysis using eq 6 (Table S9, SI).

The modified Knudsen model enables the prediction of gas permeation behavior based on the size of the target gas and its default channel diameter according to the ease of channel deformation. Although the diffusivity for every gas species would become higher for a more elastic channel, when considering the necessary requirements for H_2 separation by a molecular sieving mechanism from a H_2/CO_2 gas mixture,[21] the area can be divided into three regions (I–III) by two threshold curves for H_2 or CO_2 permeation. These curves are derived from the relationship of $d + \alpha = \sigma$ with σ_{H2} or σ_{CO2},[22] which represent a tendency to decrease with a decrease in material elasticity for each gas permeation described (Figure 3). For an example of H_2 and CO_2, the gas permeation of H_2 and CO_2 are prevented together in barrier region I and allowed in competition region III.

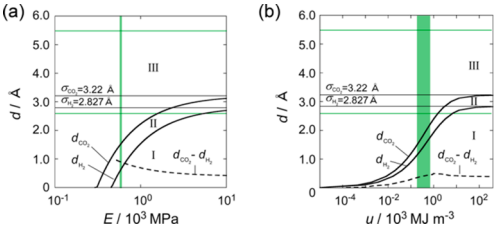

Figure 3. Threshold channel diameter of gas permeation for CO_2 (upper solid curve) and H_2 (lower solid curve) at 293 K calculated based on (a) elastic model (eq 4 with σ fixed parameter) and (b) volumetric energy model (eq 6 with σ fixed parameter), respectively. The separated areas are different characteristics of gas permeability: I, none; II, only H_2; III, both H_2 and CO_2. The curves for threshold channel diameter were derived from the relationship of $d + \alpha(\sigma) = \sigma$ with σ_{H2} or σ_{CO2}. The dotted curves in the figures are vertical widths between the threshold diameters for CO_2 and H_2. (The vertical green lines indicate best-fit E and u values in Figure 2a. The horizontal green lines indicate d^{min} for **1** (lower line) and **2** (upper line).).

dx.doi.org/10.1021/ja501045u | J. Am. Chem. Soc. 2014, 136, 6806–6809

In region II, which is between the threshold curves for CO_2 and H_2, there is a gas permeable region at $d = 0$ in the elastic model, and selective H_2 permeation would be permitted even for a nonporous membrane with adequate elasticity. From the elastic model, selective H_2 permeation can be expected for a minimum channel diameter of 0.5−1.8 Å in the single-crystal membranes of **1** and **2** with their elasticity of E = 540 MPa in fitting the curve (100−200 MPa in compression test), which is as elastic as low density polyethylene (E = 110−450 MPa).[23] The H_2 permeability of polyethylene (4.73×10^{-16} mol m m^{-2} s^{-1} Pa^{-1}) with $F\alpha_{polyethylene}$ of 1.2 for H_2/CO[24] is about 2500 times smaller by permeability and 6−20 times smaller by permselectivity than those of **1** and **2**. Thus, elasticity and regularity of pores most likely contribute to high permselectivity with high diffusivity. In the volumetric energy model, which correctly reproduced the gas permeation results, three regions (I−III) exist for the entire range of u. The vertical width of region II has a maximum positioning around the u value of **1** and **2**. Hence, materials that have similar solid characteristics with a pore diameter of 1.2−1.9 Å would be expected to show the property of selective H_2 permeation.

In conclusion, gas permeation through a channel was experimentally proved by the relationship between crystal orientation and gas permeability for the novel molecular crystal of $[Cu(II)_2(4\text{-F-bza})_4(2\text{-mpyz})]_n$ (**1**). The high performance in permeating gas was quantitatively explained by a modified Knudsen equation with the introduction of a channel space expansion induced by the gas inside, which is related to the elasticity of the channel solid. The best fit was obtained using a volumetric energy model that has the same equation formula as that of classical blackbody radiation theory.[25] The order of channel expansion magnitude in $H_2 > Ar > CH_4$ was verified by single-crystal X-ray structural analysis. Selective gas permeation without any decrease in diffusivity would be achieved indicated by designing adequate channel diameter and elasticity. This work provides a novel strategy for efficient H_2 gas purification.

■ ASSOCIATED CONTENT

Ⓢ Supporting Information

Experimental details and crystallographic data. This material is available free of charge via the Internet at http://pubs.acs.org.

■ AUTHOR INFORMATION

Corresponding Author

staka@yokohama-cu.ac.jp

Notes

The authors declare no competing financial interest.

■ ACKNOWLEDGMENTS

This work was partially supported by a Grant-in-aid for Fundamental Scientific Research (B) (No. 23350028) for S.T. and a Grant-in-aid for JSPS fellows (No. 24-10567) for Y.T.

■ REFERENCES

(1) Pandey, P.; Chauhan, R. S. *Prog. Polym. Sci.* **2001**, *26*, 853−893.

(2) Ulbricht, M. *Polymer* **2006**, *47*, 2217−2262.

(3) Ramachandran, R.; Menon, R. K. *Int. J. Hydrogen Energy* **1998**, *23*, 593−598.

(4) Robeson, L. M. *J. Membr. Sci.* **2008**, *320*, 390−400.

(5) (a) Ge, L.; Zhou, W.; Rudolph, V.; Zhu, Z. *J. Mater. Chem. A* **2013**, *1*, 6350−6358. (b) Takamizawa, S.; Kachi-Terajima, C.; Kohbara, M.; Akatsuka, T.; Jin, T. *Chem.—Asian J.* **2007**, *2*, 837−848.

(6) (a) Pinnau, I.; Casillas, C. G.; Morisato, A.; Freeman, B. D. *J. Polym. Sci. Polym. Phys.* **1996**, *34*, 2613−2621. (b) Du, N.; Park, H. B.; Robertson, G. P.; Dal-Cin, M. M.; Visser, T.; Scoles, L.; Guiver, M. D. *Nat. Mater.* **2013**, *10*, 372−375.

(7) (a) Shao, L.; Low, B. T.; Chung, T. S.; Greenberg, A. R. *J. Membr. Sci.* **2009**, *327*, 18−31. (b) Carta, M.; Malpass-Evans, R.; Croad, M.; Rogan, Y.; Jansen, J. C.; Bernardo, P.; Bazzarelli, F.; McKeown, N. B. *Science* **2013**, *339*, 303−307.

(8) (a) De Vos, R. M.; Verweij, H. *Science* **1998**, *279*, 1710−1711. (b) Yin, X.; Zhu, G.; Yang, W.; Li, Y.; Zhu, G.; Xu, R.; Sun, J.; Qiu, S.; Xu, R. *Adv. Mater.* **2005**, *17*, 2006−2010. (c) Lu, G. Q.; Diniz da Costa, J. C.; Duke, M.; Giessler, S.; Socolow, R.; Williams, R. H.; Kreutz, T. *J. Colloid Interface Sci.* **2007**, *314*, 589−603. (d) Guerrero, V. V.; Yoo, Y.; McCarthya, M. C.; Jeong, H. K. *J. Mater. Chem.* **2010**, *20*, 3938−3943.

(9) Talu, O.; Sun, M.; Shah, D. B. *AIChE J.* **1998**, *44*, 681.

(10) Takamizawa, S.; Takasaki, Y.; Miyake, R. *J. Am. Chem. Soc.* **2010**, *132* (9), 2862−2863.

(11) Introducing 2-methylpyrazine vapor (0.58 g, 6.2 mmol) into the methanol solution (200 mL) of copper(II) acetate monohydrate (0.30 g, 1.5 mmol) and 4-fluorobenzene (2.23 g, 15.9 mmol) gave blue single crystals of **1** with a size of 100−500 μm in 38% yield (443 mg). Well-formed single crystals were used after vacuum-dry at 298 K.

(12) (a) Takamizawa, S.; Nakata, E.; Yokoyama, H. *Inorg. Chem. Commun.* **2003**, *6*, 763−765. (b) Takamizawa, S.; Saito, T.; Akatsuka, T.; Nakata, E. *Inorg. Chem.* **2005**, *44*, 1421−1424.

(13) Single-crystal X-ray structural analysis of **1** was performed at 90 K on a Bruker Smart APEX CCD area diffractometer (Bruker AXS) with a nitrogen-flow temperature. Crystal data for **1** at 90 K: monoclinic, $C2/m$, a = 16.7561(17) Å, b = 9.7376(11) Å, c = 11.7980(12) Å, $\alpha = 90°$, β = 118.328(2)°, $\gamma = 90°$, V = 1694.0(3) Å^3, $Z = 2$, D_{calc} = 1.524 Mg m^{-3}, R_1 = 0.0463 (0.0610), wR_2 = 0.1318 (0.1466) for 1535 reflections with $I > 2\sigma(I)$ (for 1833 reflections (5471 total measured)), goodness-of-fit on F^2 = 1.123, largest diff peak (hole) = 1.060 (−1.002) e Å^{-3} (CCDC-983937).

(14) Poling, B. E.; Prausnitz, J. M.; O'Connell, J. P. *The Properties of Gases and Liquids*, 5th ed.; McGraw-Hill: New York, 2000.

(15) Only CO_2 was treated as the smallest gas except for H_2 and He based on the minor radius of the CO_2 molecule, which gave a reasonable permeation order in the analysis, although the Lennard-Jones diameter of CO_2 is the largest in this study (Table S5, SI).

(16) Seader, J. D.; Henley, E. *Separation Process Principles*; John Wiley & Sons, Inc.: New York, 1998.

(17) This tendency did not obey the expectation that f_{obs} became invariant for every gas species in eqs 1 and 2 (Figure 2a). In addition, f_{obs} for H_2 was far above the calculated flat line of f_{calc} (black dotted line in Figure 2a) due to the unexpected high H_2 gas permeability of **1**.

(18) The effective channel diameter ($d^*(\sigma)$) and porosity (ε^*) are derived as, $d^*(\sigma) = ((d + \alpha)^2 - \sigma^2)^{1/2}$ and $\varepsilon^* = \varepsilon(d + \alpha)^2/d^2$.

(19) Because d_1^{max} and d_2^{max} are almost the same values of d_1^{min} and d_2^{min} are expected to be sensitive to the curve of $f(\sigma)$. In fact, the correct value can be obtained by adopting d^{min} in seeking a physically feasible $f(\sigma)$ because the decreased tendency of f_{obs} cannot be represented by adopting d^{max} or the mean value of d^{max} and d^{min} for any value of α. (Figure S6, SI)

(20) These experimental values of E for **1** and **2** (298 K) are $10-10^2$ times smaller than the values for a single crystals of zeolite (ZSM-5) and rigid MOFs (MOF-5 and HKUST-1) (Table S8, SI).

(21) Because of the order of He < H_2 < CO_2 < others for gas molecular diameter, the required channel diameter and its elasticity for the selective H_2 permeation from H_2/CO_2 can guarantee the sieving permeation of H_2 out of any gas mixtures containing H_2 except for He.

(22) The value of α was calculated with σ_{H2} or σ_{CO2} by regarding E or u as variable in eq 4 or eq 6, respectively.

(23) Matweb. Retrieved Feb 7, 2013.

(24) Covarrubias, C.; Quijada, R. *J. Membr. Sci.* **2010**, *358*, 33−42.

(25) Planck, M. *Vorlesungen über die Theorie der Wärmestrahlung*; Johann Ambrosius Barth: Leipzig, 1906.